Environment International 133 (2019) 105204

Contents lists available at ScienceDirect

Environment International

journal homepage: www.elsevier.com/locate/envint

Catalytic pyrolysis of swine manure using CO_2 and steel slag

Dong-Jun Lee[a,b], Kwang-Hwa Jeong[b], Dong-Hyun Lee[b], Sung-Hyoun Lee[b], Min-Woong Jung[b], Yu-Na Jang[b], Gwang-Gon Jo[b], Jung Hoon Kwag[b], Haakrho Yi[c], Young-Kwon Park[d,*], Eilhann E. Kwon[a,*]

[a] Department of Environment and Energy, Sejong University, Seoul 05005, Republic of Korea
[b] Department of Animal Environment, National Institute of Animal Science (NIAS), Wanju 55365, Republic of Korea
[c] Gwangyang Research Group, Research Institute of Industrial Science and Technology, Gwangyang 37673, Republic of Korea
[d] School of Environmental Engineering, University of Seoul, Seoul 02504, Republic of Korea

ARTICLE INFO

Keywords:
Livestock manure
Swine manure
Waste-to-energy
Pyrolysis
Carbon dioxide
Catalysis

ABSTRACT

Pyrolysis of swine manure (SM) was conducted as a case study to establish an environmentally sound management of livestock manure. To build a more renewable pyrolysis platform for SM, this study selected carbon dioxide (CO_2) as the reaction medium. In addition, CO_2 was used in pyrolysis of SM to restrict the formation of toxic compounds, such as benzene derivatives and polycyclic aromatic hydrocarbons (PAHs). A series of thermogravimetric analysis (TGA) tests was done to understand the thermolysis of SM in the CO_2 environment. The TGA tests elucidated no occurrence of heterogeneous reactions between the SM sample and the CO_2. Moreover, the TGA tests of SM suggested that SM contains more volatile matter (VM) than lignocellulosic biomass. Non-catalytic transesterification of SM lipids confirmed that the dried SM sample contained 8.85 ± 0.05 wt% of lipids. This study also confirmed that the mechanistic role of CO_2 was realized through the gas phase reactions between volatile pyrolysates evolved from the thermolysis of SM and CO_2. In summary, CO_2 donates O, enhancing the generation of CO through homogeneous reactions. In parallel, this study confirmed that CO_2 suppress dehydrogenation. Therefore, the identified gas phase reactions between volatile pyrolysates and CO_2 led to the compositional modifications in the condensable pyrolysates. However, such mechanistic features arising from CO_2 only initiated at ≥520 °C. To expedite the reaction kinetics of the homogeneous reaction triggered by CO_2, steel slag (SS) was used as a catalyst. Hence, the reaction kinetics associated with the mechanistic role of CO_2 were substantially enhanced (up to 80%) when SS was used as a catalyst. Therefore, all experimental findings strongly suggest that CO_2 can be utilized as a raw material in a thermo-chemical process. More importantly, all observations suggest that CO_2 lopping can also be achieved in a thermo-chemical process. Lastly, this study shows that the high Cu content in SM was effectively immobilized through pyrolysis. Conclusively, this study experimentally proved that CO_2 could be promising for restricting the formation of toxic pollutant in the thermo-chemical treatment in that CO_2 offers an innovative and strategic means for controlling the ratio of C to H. Note that aromaticity and toxicity of chemical compounds are highly contingent on the ratio of C to H.

1. Introduction

According to the International Energy Agency (IEA), the global energy consumption was equivalent to 14 billion tons of oil equivalent in 2018, nearly two times higher the consumption in 2010 (Bilgen, 2014; Cséfalvay and Horváth, 2018). Considering that fossil fuels support 80% of the global energy demand, this heavy reliance accelerates global warming (Meinshausen et al., 2009). Global CO_2 emissions from combustion of fossil fuels reached 33 Gt in 2018, which exceeds the planet's full capacity to assimilate carbons through the natural carbon cycle, which results in the atmospheric concentration of CO_2 (Cséfalvay and Horváth, 2018; Stier et al., 2019). Based on the national oceanic and atmospheric administration (NOAA) report, the global average atmospheric CO_2 in 1980 and 2017 were 330 and 405 ppm, respectively (Hashimoto, 2019). In addition, CO_2 levels today are higher than at any point in at least the past 800,000 years because the anthropogenic carbon inputs are exceeding the planet's carbon sequestration capacity (Hashimoto, 2019). To delay and mitigate the ecological perturbations by the surplus amount of CO_2 (Wigley and Raper, 1987), numerous researches on sustainable energy have been done over the last two

* Corresponding authors.
E-mail addresses: catalica@uos.ac.kr (Y.-K. Park), ekwon74@sejong.ac.kr (E.E. Kwon).

https://doi.org/10.1016/j.envint.2019.105204
Received 23 May 2019; Received in revised form 18 September 2019; Accepted 19 September 2019
Available online 19 October 2019

decades (Dhillon and von Wuehlisch, 2013; Stier et al., 2019).

In this context, carbon neutral/free renewable energies (e.g., bioethanol, biodiesel, biohydrogen, wind power, hydraulic power, photovoltaic, solar thermal energy, geothermal energy, *etc*.) have gained considerable attention from both the academia and the industry (Bortolini et al., 2014; Jung et al., 2016; Kabalci, 2013; Lee et al., 2016; Zabed et al., 2017). Meanwhile, the public acceptance of sustainable energy use has been further developed. Accordingly, the use of renewable energies has been mandatorily promoted by legislative enactments including the renewable fuel standard (RFS) and the renewable portfolio standard (RPS) (Balan et al., 2013; Huh et al., 2015). Among renewable energies, the practical implementation of biofuels has been established due to their high compatibility with current energy/chemical infrastructures (Lardon et al., 2009). In detail, biofuels can be directly used by blending with gasoline and diesel without any engine modifications (Lardon et al., 2009). Furthermore, they can share the distribution network of fossil fuels (Lardon et al., 2009). More importantly, converting biomass into biofuels is regarded as an initial step for biorefinery (Fatih Demirbas, 2009; Li and Hu, 2016; Nizami et al., 2017). Therefore, biomass can be further processed as a raw material to produce the valuable chemicals via the consecutive unit operations with/without the catalytic applications (Sheldon, 2017). Nonetheless, the insecure supply chain of biomasses is one of the major obstacles for the further expansion of its use as raw material for biofuels and biorefinery (Ghaderi et al., 2016; Li and Hu, 2016; Varun et al., 2009). That insecurity can be attributed to regional and seasonal variations (Ghaderi et al., 2016). Furthermore, the use of edible crops as raw feedstock for biofuel and biorefinery can have several negative consequences, such as water shortage, ethical dilemma (Tomei and Helliwell, 2016).

In these regards, it is desirable to recover energy and valuable resource from waste materials based on the concept of waste-to-energy (WtE) and biorefinery (Sheldon, 2017). For example, the use of livestock manure as a carbonaceous material can be a viable option (Awasthi et al., 2019; Burra et al., 2016; Fuchsz and Kohlheb, 2015; Hussein et al., 2017; Kahiluoto et al., 2015; Xin et al., 2017; Yuan et al., 2017). The global demand for proteins in line with our economic growth has rapidly increased (Fuchsz and Kohlheb, 2015). Livestock is housed in closed quarters or outside in feedlots for mass livestock production (Awasthi et al., 2019). This situation generates concern regarding the environmental burdens of livestock (Fuchsz and Kohlheb, 2015), and manure management has been perceived as one of the critical environmental issues (Fuchsz and Kohlheb, 2015; Prosser and Sibley, 2015). Manure can be used as fertilizer (Chen et al., 2019; Kahiluoto et al., 2015; Lee et al., 2018). However, the amount of inorganic nutrients (P and N) practiced to arable land from manure compost has begun to exceed the requirement for crop growth and lead to water contamination owing to surface runoff (Kahiluoto et al., 2015; Lee et al., 2018). As a result, it is pertinent to improve livestock manure management (Awasthi et al., 2019; Burra et al., 2016; Hussein et al., 2017; Xin et al., 2017; Yuan et al., 2017).

Among various technical routes, the thermo-chemical process (pyrolysis and gasification) of livestock manure is likely a viable technical alternative since it is insensitive to physico-chemical properties of carbon substrates compared to other fuel processing technologies (Awasthi et al., 2019; Burra et al., 2016; Hussein et al., 2017; Xin et al., 2017; Yuan et al., 2017). Gasification is referred to as "*converting the heating value of solid carbonaceous materials into the combustible syngas*" (Awasthi et al., 2019; Burra et al., 2016; Fatih Demirbas, 2009; Hussein et al., 2017; Li and Hu, 2016; Sansaniwal et al., 2017; Xin et al., 2017). The syngas generated from the gasification process can be used directly as a fuel or as an initial feedstock for chemical synthesis (Awasthi et al., 2019; Fatih Demirbas, 2009; Li and Hu, 2016). Pyrolysis is referred to as "*redistributing carbons in the carbon substrates into three pyrogenic products (syngas, pyrolytic oil, and char) in an oxygen-free environment*" (Mishra and Mohanty, 2018; Yuan et al., 2017). Given that pyrolysis is the intermediate step for gasification, all mechanistic understanding of the pyrolysis process can be directly applied to the gasification process (Nizami et al., 2017; Oh et al., 2017; Xin et al., 2017).

Based on these rationales, this study mainly focused on the pyrolysis of livestock manure. For livestock housed in closed quarters, livestock manure is an economically viable waste material because a large amount can be easily gathered from a single site. It is of note that biomass transport and energy recovery are costly steps of this process (Nizami et al., 2017). Therefore, this study on pyrolysis of swine manure (SM) was conducted as a case study. To establish a more sustainable pyrolysis platform, CO_2 was used as the reactive gas medium. Also, the use of CO_2 during pyrolysis of SM was considered in that we assume that CO_2 offered an innovative and strategic way to restrict the formation of toxic chemical compounds, such as benzene derivatives and PAHs. In particular, we laid the great efforts to convert CO_2 into fuel to achieve the ultimate carbon management. As such, the thermolysis of SM in a CO_2 environment was investigated at fundamental levels. To this end, a series of thermo-gravimetric analysis (TGA) was conducted in a CO_2 environment. The pyrogenic products were characterized to clarify the mechanistic roles of CO_2. All data interpretations were performed in reference to the thermolysis of SM in an inert (N_2) condition. Lastly, steel slag (SS) was employed as a catalytic material to increase the mechanistic effects of CO_2. The use of SS was aimed to catalytically increase the reaction kinetics associated with the CO_2 in pyrolysis of SM. Furthermore, the exploitation of SS was considered because the significant amount of SS was inevitably generated from steelworks, but the practical implementation of it as a cheap catalyst has not been fully investigated. Indeed, to our best knowledge, CO_2-cofeeding pyrolysis of SM using SS has not been found elsewhere. Furthermore, we assumed that the identified mechanistic roles of CO_2 from this study could be directly applied in air pollution controls because the present study laid great emphasis on the reactions of volatile organic compounds (VOCs) and CO_2.

2. Materials and methods

2.1. Sample preparation and chemical agents

The SM samples were collected from a pig barn in Cheonan, Korea. They were dried at 80 °C for 2 d to remove moisture. The samples were milled with a ball mill, and their average size was adjusted to ≤600 μm. The elemental analysis was performed using an organic elemental analyzer (Vario MACRO cube, Elementar Analysensysteme GmbH, Germany). The results showed 42.18 wt% of C, 47.98 wt% of O, 6.28 wt % of H, 2.65 wt% of N, and 0.91 wt% of S in the SM. Moreover, non-catalytic transesterification was done to quantify the total lipid content in the SM and specify the compositional matrix of lipids (i.e., fatty acid profiles). All conversion parameters for non-catalytic transesterification was based in our previous work (Jung et al., 2016; Lee et al., 2016). The SS used in this study was collected from POSCO Steel Works, in Korea. The metal speciation of SS, given by POSCO, is summarized in Table 1. Other products, namely methanol (≥99.9%) (Prod. # 34860), dichloromethane (≥99.9%) (Prod. # 270997), nitric acid (≥70%) (Prod. # 348073), and silica (Prod. # 243981), were purchased from Sigma-Aldrich (St. Louis, MO, USA). Ultra-high purity gases (≥99.999), N_2 and CO_2, were purchased from AirTech Korea (Seoul, Korea).

2.2. Thermo-gravimetric analysis (TGA) of swine manure in the CO_2 environment

A series of TGA tests was conducted to figure out the thermolytic behavior of SM in various atmospheric conditions. All TGA tests were conducted using a Netzsch TGA unit (STA 449 F5 Jupiter, Germany), and all experimental parameters for the TGA tests were the same. For that, 10 ± 0.01 mg of dried SS were thermally decomposed at a heating rate of 10 °C/min from 20 to 900 °C, and mass decay as a

Table 1
Metal speciations in steel slag (SS).

Metal species	Content (wt.%)
Na	0.20
Mg	3.12
Al	8.15
Si	12.70
P	0.27
S	5.27
Cl	0.14
K	0.05
Ca	65.10
Ti	0.14
V	0.05
Cr	0.02
Mn	0.26
Fe	4.49
Cu	0.01
Zn	0.01
Sr	0.03
Ba	0.02

function of the experimental temperatures was digitally recorded. Prior to each TGA test, the reference test (i.e., no sample loading) was performed to eliminate the buoyancy effects of purge and protective gases. Note that the buoyancy effects are attributed to the density variations of purge (20 mL/min) and protective gases (50 mL/min). These flow rates were automatically controlled by imbedded mass flow controllers (MFCs) in the TGA unit. The imbedded MFCs were certified by the TGA manufacturer (Netzsch, Germany).

2.3. Lab-scale pyrolysis of SM using a tubular reactor in a CO_2 environment

A batch-type fixed-bed tubular reactor was assembled. A quartz tubing (Chemglass CGQ-0800T-68) was selected as the main body of the tubular reactor to exclude the catalytic effects. The dimensions of the tubular reactor were 1.2 m of length and 25.4 mm of outer diameter. To equip the gas inlet/outlet systems and record the inner temperature of the tubular reactor using a thermocouple (K-type, Omega, USA), two stainless Ultra Torr vacuum fittings (Prod. # SS-UT-6-600, Swagelok, USA) were fitted to both ends of the tubular reactor. In addition, two stainless step-down unions (25.4–6.35 mm) were directly fitted to both ends of the Ultra Torr vacuum fittings. A gas flow rate of 100 mL/min was used for N_2 and CO_2. A tubular furnace (RD 30/200/11, Nabertherm, USA) was used as an external heating source to maintain the experimental temperature. This tubular furnace consisted of two heating elements, and each of them could be controlled individually. For the one-stage pyrolysis experiment, both heating elements were controlled simultaneously, and 1.0 ± 0.01 g of dried SM was loaded at the center of the first heating element. At the two-stage pyrolysis experiment, the heating elements were controlled separately: in the first heating element a heating rate of 10 °C/min was used, and in the second heating element, isothermal conditions (650 °C) were maintained. Similarly to the one-stage pyrolysis, 1.0 ± 0.1 g of dried SM were placed in the center of the first heating element. In addition, 1.0 ± 0.1 g of powdery SS blended with silica was loaded in the center of the second heating element for the catalytic pyrolysis of SM. The gaseous effluents were condensed with a liquid nitrogen cooled trap. After the condensable hydrocarbon species were separated, the gaseous effluents from the tubular reactor were quantified using an on-line micro-gas chromatography (GC) (3000A, Inficon, Switzerland). The collected hydrocarbon species and the solid residue in the reactors were weighted to estimate the overall mass balance of the pyrogenic products. The mass portion of the pyrogenic gas was estimated by subtracting the total mass of condensable hydrocarbons and solid residue. The overall layout for the experimental setup was shown in Fig. SI-1 (Supplementary Information).

Table 2
Metal speciation in swine manure (SM).

Metal species	Content (wt.%)
Al	0.29
Ca	6.54
Cu	0.04
Fe	1.05
K	2.86
Mg	6.05
Mn	0.30
Na	0.55
Sr	0.03
Zn	0.30

2.4. Quantification, qualification, and characterization of pyrogenic products

After trapping the condensable hydrocarbon species, the gaseous effluents were quantified using a micro-GC unit, which was previously calibrated using the gas standard (Scotty Analyze Gases, Inficon, Switzerland). Moreover, trapped hydrocarbon species were identified using a GC/time-of-flight (TOF) mass spectrometer (MS) (Agilent 7850B, USA and ALMSCO Bench-Top, UK) equipped with an Elite-5MS column (30 m × 0.25 m × 0.25 μm) (Prod. # N9316282, PerkinElmer, USA). To determine the metal speciation and quantification of the dried SM and biochar, an inductively coupled plasma-optical emission spectrometer (ICP-OES) unit (Optima 5300 DV, PerkinElmer, USA) was used. Metals in SM were extracted by a microwave digestion unit (Ethos 1600, Milestone, Italy) using nitric acid. A toxicity characteristic leaching procedure (TCLP) of SM biochar was conducted under pH 4.8 and 30 rpm for 18 h (Zhou et al., 2017). The metal species in SM are summarized in Table 2.

3. Results and discussion

3.1. Characterization of the SM thermolytic behavior in a CO_2 environment

To characterize the thermolysis of SM in CO_2, 10 ± 0.01 mg of SM were thermally degraded in CO_2 at a heating rate of 10 °C/min from 20 to 900 °C. For reference, the same TGA test of SM was performed in an inert gas (N_2) environment. The mass decays of SM in N_2 and CO_2 are presented in Fig. 1(a). Their thermal degradation rates (i.e., differential thermogram: DTG) were incorporated in Fig. 1(a) to discern any differences in the thermolytic pattern of SM induced by CO_2.

As depicted in Fig. 1(a), the mass decay of SM in both environments are nearly identical at ≤748 °C. These similar thermolytic patterns in N_2 and CO_2 suggest no mechanistic influence of CO_2 on the thermolysis of SM. A similar thermolytic trend also implied no occurrence of heterogeneous reactions between the solid phase sample (SM) and CO_2, considering that heterogeneous interactions result in the different thermolytic trends. In detail, the heterogeneous reactions of SM and CO_2 result in the different thermal degradation rate of SM. Based on these facts, the similar mass decay patterns at ≤748 °C in Fig. 1(a) prove no occurrence of heterogeneous reactions. In other words, the similar thermal decomposition of SM can be interpreted as homogeneous reactions (i.e., reactions of volatile pyrolysates from the thermolysis of SM and CO_2). Considering that the TGA test is only to inform mass change as a function of thermolytic temperatures, all homogeneous reactions induced by CO_2 are evidenced by the TGA test.

At ≥748 °C, the thermal degradation rate of SM is faster in CO_2 than in N_2. In other words, the more mass conversion was achieved in the CO_2 environment due to the Boudouard reaction ($C(S) + CO_2 \rightleftharpoons 2CO$). Indeed, the Boudouard reaction is thermodynamically favorable at ≥710 °C (Jang et al., 2016). However, mass decay of SM continuously occurs from 748 to 900 °C, even in N_2. Therefore, mass decay of SM in

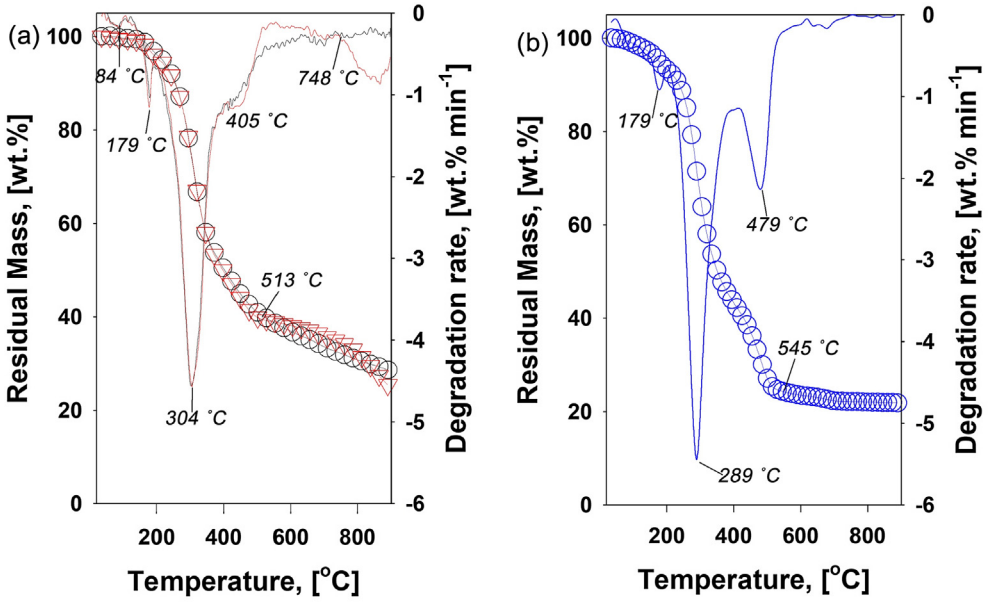

Fig. 1. (a) Mass decay of SM as a function of the thermolytic temperatures in N_2 (black color) and CO_2 (red color) and its thermal degradation rates, (b) Mass decay of SM in air (blue color) and its thermal degradation rate. (For interpretation of the references to colour in this figure legend, the reader is referred to the web version of this article.)

CO_2 at ≥748 °C is not solely attributed to the Boudouard reaction. Fig. 1(a) also demonstrates that the reaction kinetics of the Boudouard reaction at ≥748 °C are not fast. Hence, the final residual mass in the CO_2 environment is not much different from that in the N_2 environment. For example, despite occurrence of the Boudouard reaction, the reaction kinetics of it does not contribute the discernible final residual mass. For comparison, the same TGA test of SM was conducted in an air environment. The mass loss and thermal degradation rate of SM are presented in Fig. 1(b). As shown in Fig. 1(a) and (b), the final mass in air is not significantly different from that in N_2 and CO_2. Two conclusions can be drawn from this observation. First, the final residual mass of SM in reference to lignocellulosic biomass is not substantial. In other words, SM contains a large amount of volatile matter (VM). Second, the reaction kinetics of the Boudouard reaction are not fast enough to consume all carbons in the biochar. Considering that the heating rate of the TGA test was 10 °C/min and the Boudouard reaction initiated at ≥748 °C, the conversion of carbon from the biochar into CO by the Boudouard reaction is not completed within 15 min.

3.2. Lab-scale pyrolysis of SM in the CO_2 environment

A series of the TGA tests in Fig. 1(a) experimentally evidenced no occurrence of homogenous reactions at ≤748 °C. Moreover, the TGA tests did not elucidate the occurrence of homogeneous reactions (among volatile pyrolysates from the thermolysis of SM and CO_2). To confirm the homogeneous reactions, lab-scale pyrolysis of SM was performed using a batch-type fixed-bed tubular reactor. In detail, 1 ± 0.01 g of SM was loaded in the tubular reactor, and the pyrolysis was conducted at a heating rate of 10 °C/min from 20 to 720 °C. The highest temperature (720 °C) was determined to exclude any effects arising from the Boudouard reaction, which initiates at ≥748 °C as shown in Fig. 1(a). Assuming that CO_2 has a role during the thermolysis of SM, the overall mass balance of three pyrogenic products are essential to evidence the homogeneous reactions. In summary, except for the mass portion of biochar, the mass portions of pyrolytic oil and pyrolytic gas in CO_2 must be different from those in N_2 due to the homogeneous reactions between volatile pyrolysates and CO_2. To confirm this hypothesis, the overall mass balance of three pyrogenic products from pyrolysis of SM at a heating rate of 10 °C/min from 20 to 720 °C in N_2 and CO_2 are established in Fig. 2(a).

The mass portions indicating the final residues (biochar) generated from the N_2 and CO_2 environments are not much different (Fig. 2(a)), which is consistent with the TGA results from Fig. 1(a). Fig. 2(a) also demonstrates that the more gaseous pyrolysates are generated in CO_2. In contrast, a lower amount of liquid pyrolysates is generated in CO_2. Accordingly, the different mass content of gaseous and liquid pyrogenic products in Fig. 2(a) is an evidence for the homogeneous reactions. Nonetheless, the difference in the mass content of gaseous and liquid pyrolysates arising from CO_2 is not substantial. This implies that the reaction kinetics of the homogeneous reactions are not fast to differentiate the mass portion for each pyrolysate. To investigate further, the collected pyrolytic oil was diluted with the same amount of dichloromethane. Subsequently, the compositional matrix of the pyrolytic oil was determined using a GC/TOF-MS unit, and their identifications can be visualized in the chromatogram of Fig. 2(b). The major chemical species in Fig. 2(b) were labelled, and their peak areas are summarized in Table 3.

In Table 3, it can be observed that the compositional matrix of condensable pyrolysates in CO_2 is different from that in N_2. Despite that CO_2 is essential to modify the compositional matrix of condensable pyrolysate, the precise mechanisms on CO_2 cannot be elucidated. Nonetheless, Fig. 2(a) and Table 3 show that the peak areas of most phenolic compounds decreased in CO_2. Such phenomena suggest that CO_2 suppress dehydrogenation, considering that dehydrogenation offers a favorable condition for the formation of benzene derivatives including phenolic compounds (Kwon et al., 2015; Oh et al., 2017). More importantly, the identified phenomena (suppressed dehydrogenation by CO_2) offered a principle strategy for restricting the formation of toxic chemical compounds, such as benzene derivatives and PAHs. Fig. 2(b) and Table 3 also show that the major constituents of condensable pyrolysates are aliphatic hydrocarbons. Particularly, there was a large amount of C15-18 aliphatic hydrocarbons and fatty acids in the pyrolytic oil. Accordingly, identification of such chemical species strongly suggest that SM contains a large amount of lipids (Oh et al., 2017).

To quantify the total lipid content in the SM sample, non-catalytic transesterification of the lipids extracted from the dried SM was conducted. The presence of fatty acid methyl esters (FAMEs) can be visualized through the chromatogram in Fig. 3. The total lipid content and speciation of the SM sample are summarized in Table 4. As depicted in Fig. 3 and summarized in Table 4, lipids in SM mostly comprise C14-18 fatty acids, and the lipid content of the SM sample is equivalent to 8.85 ± 0.05 wt%. Accordingly, the high content of fatty acids and aliphatic hydrocarbons in condensable pyrolysates is mainly attributed to the large amount of lipids in SM. Lipids (i.e., triglycerides: TGs) do

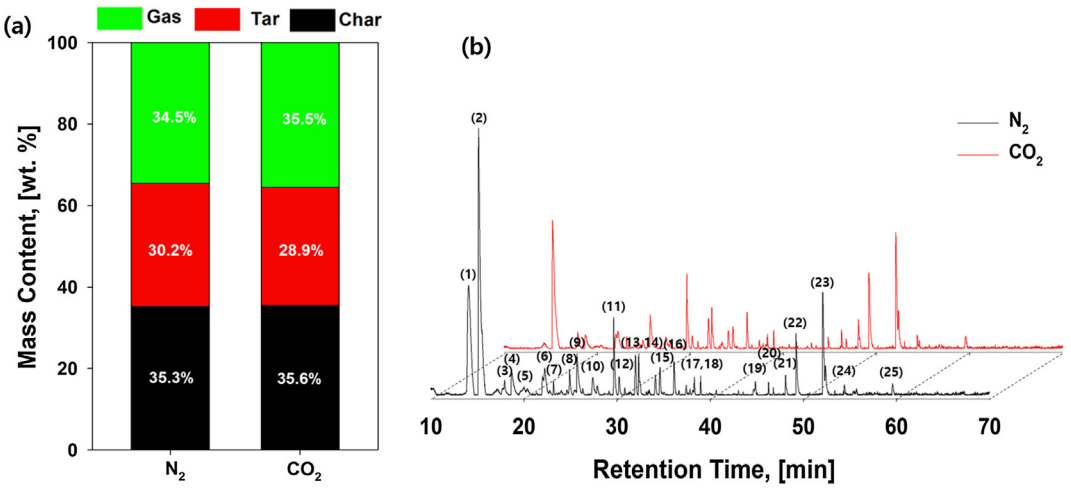

Fig. 2. (a) Overall mass balance of three pyrogenic products evolved from pyrolysis of SM in the N_2 and CO_2 environments, (b) Identification of the chemical species in pyrolytic oil generated from pyrolysis of SM in the N_2 and CO_2 environments.

not have a boiling point (T_b) (Jung et al., 2016; Lee et al., 2017; Lee et al., 2016), and the thermal degradation of TGs is generally initiated by bond dissociations of fatty acids from the triglyceride backbone (Jung et al., 2016; Lee et al., 2017; Lee et al., 2016). In fatty acids, the thermal stability of the carboxyl group is inferior to that of the long carbon chain hydrocarbon fraction (Kwon et al., 2012). This inferior thermal stability results in the formation of C15-18 aliphatic hydrocarbons in the condensable pyrolysate. Furthermore, the thermal cracking of fatty acids provides favorable conditions to form benzene derivatives (Kwon et al., 2012; Oh et al., 2017). Nonetheless, the peak areas of C15-18 fatty acids in the CO_2 environment are larger than those in the N_2 environment. This observation also suggests that CO_2 likely suppresses dehydrogenation. Moreover, the high content of lipids in SM is consistent with the experimental observations from the TGA test (Fig. 1). The final residual mass of SM from the TGA tests was relatively lower than that of lignocellulosic biomass (Mishra and Mohanty, 2018).

To further investigate the mechanistic role of CO_2, the gaseous effluents from the pyrolysis of SM in N_2 and CO_2 environments were compared as a function of thermolytic temperatures, as shown in Fig. 4. The gas evolution patterns in N_2 may well reflect a typical thermolytic trend for biomass. For instance, H_2 evolution through dehydrogenation is proportional to the thermolytic temperatures, and this evolution trend can be observed in Fig. 4. The formation of H_2 initiated at $\geq$480 °C and reached the highest value at 650 °C. At $\geq$650 °C, the concentration of H_2 began to decrease, likely due to the depletion of H_2

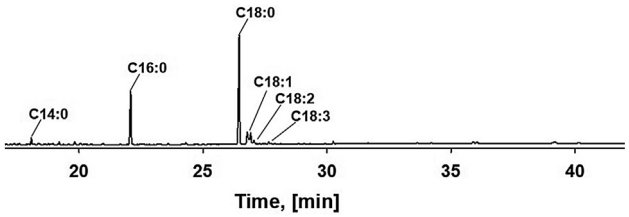

Fig. 3. Identification of fatty acids derived from non-catalytic transesterification of lipid extracted from the SM sample.

Table 3
Identification of the chemical species in pyrolytic oil generated from pyrolysis of SM in N_2 and CO_2.

No.	Retention time, [min]	Compound	Peak area from N_2	Peak area from CO_2	Peak area difference (%)
1	14.305	toluene	72,823,288	4,003,735	−94.50
2	15.122	acetic acid	113,875,508	57,285,996	−49.69
3	17.920	methacrylonitrile	6,147,016	4,401,270	−28.40
4	18.672	propanomic acid	11,254,541	6,174,451	−45.14
5	20.003	styrene	5,531,471	N.D.	N/A
6	21.993	butanoic acid	4,901,038	3,307,389	−32.52
7	23.168	furfuryl alcohol	2,022,734	1,625,792	−19.62
8	24.921	pentanoic acid	5,653,746	2,311,857	−59.11
9	25.688	acetamide	14,143,387	10,119,574	−28.45
10	27.867	1-dodecene	2,619,155	1,921,155	−26.65
11	29.644	phenol	15,963,687	13,388,789	−16.13
12	30.828	3-methyl-phenol	1,030,643	1,109,024	7.61
13	31.960	pentadecane	9,165,234	6,842,955	−25.34
14	32.322	4-methyl-phenol	8,416,902	7,068,368	−16.02
15	34.108	hexadecane	4,300,894	3,954,555	−8.05
16	36.115	heptadecane	6,838,233	7,269,106	6.30
17	38.300	2,5-pyrrolidinedione	2,377,289	2,113,168	−11.11
18	38.968	1H-indole	2,047,063	1,825,216	−10.84
19	44.831	heptadecanenitrile	2,773,643	1,555,170	−43.93
20	46.259	methyl pentadecanoate	1,835,367	2,388,693	30.15
21	48.086	nonadecanenitrile	3,862,011	6,217,221	60.98
22	49.217	hexdecanoic acid	14,544,934	19,591,008	34.69
23	52.093	octadecanoic acid	22,111,918	25,769,073	16.54
24	54.404	nonanamide	1,790,360	2,205,512	23.19
25	59.568	octanamide	2,814,500	3,323,724	18.09

Table 4
Total lipid content in the SM sample and the composition matrix of fatty acid in lipid extracted from the SM sample.

Lipid content	C14:0	C16:0	C18:0	C18:1	C18:2	C18:3
[wt.%]	Mass of fatty acid, [wt.%]					
8.85 ± 0.05	2.37 ± 0.01	25.36 ± 0.16	54.29 ± 0.07	16.43 ± 0.13	1.07 ± 0.16	0.8 ± 0.20

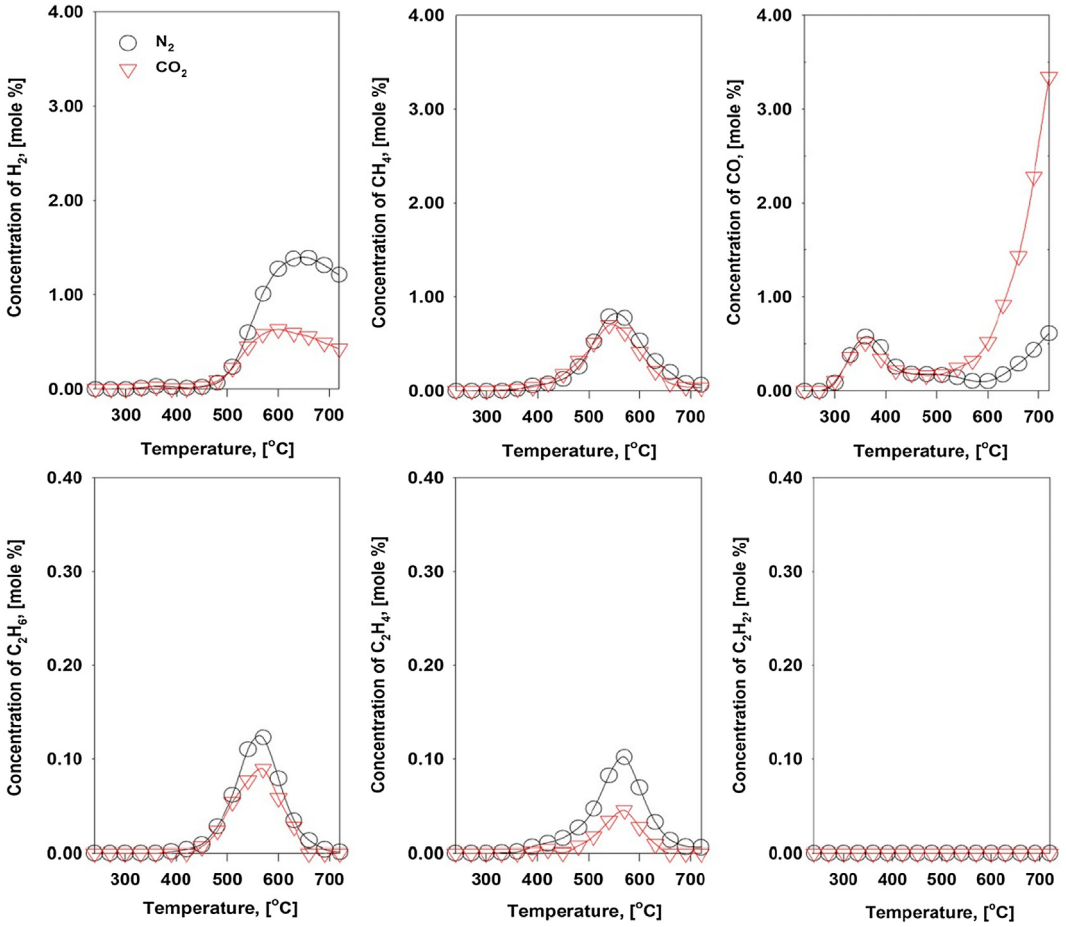

Fig. 4. Concentration profiles of H_2, CH_4, CO, C_2H_6, C_2H_4, and C_2H_2 from pyrolysis of SM in N_2 (black color) and CO_2 (red color) (Pyrolysis of SM (1.0 ± 0.01 g) is conducted at a heating rate of 10 °C min^{-1} from 20 to 720 °C). (For interpretation of the references to colour in this figure legend, the reader is referred to the web version of this article.)

in the batch-type pyrolysis experiment. The generation of CO by the pyrolysis of SM began at ≥300 °C. The formation mechanism of CO is mainly attributed to bond dissociations of CO from the polymeric backbone of SM. The formation mechanism of C1-2 hydrocarbons (CH_4, C_2H_6, and C_2H_4) are also the same as that of CO.

However, the gaseous effluents from the pyrolysis of SM in the CO_2 environment do not follow a typical thermolytic trend. For instance, the concentration of CO begins to increase at ≥520 °C. Such enhanced generation of CO is proportional to the thermolytic temperatures, shown in Fig. 4. As noted, the Boudouard reaction initiates at ≤748 °C, which was experimentally proved via a series of the TGA tests of SM in Fig. 1. Therefore, the enhanced generation of CO is likely due to the homogeneous reactions between volatile pyrolysates and CO_2. In summary, CO_2 provides O to form CO through homogeneous reactions. However, the precise mechanisms on how CO_2 can be an O donor is not clear. One of the most interesting observations in Fig. 4 is that the temperature regime exhibiting the enhanced generation of CO and the suppressed generation of H_2 nearly overlap, which can be considered an essential evidence of the dehydrogenation suppression induced by CO_2.

3.3. Two-stage and catalytic pyrolysis of SM in the CO_2 environment

All experimental findings from Figs. 2 to 4 did not fully elucidate the reactions between volatile pyrolysates and CO_2 because the observed CO_2 effects on the thermolysis of SM were limited at ≥520 °C. As evidenced by the mass decay of SM from a series of TGA tests (Fig. 1), the major thermal degradation providing volatile pyrolysates was completed at ≤520 °C. Therefore, it is desirable to understand why the enhanced generation of CO and suppressed dehydrogenation did not initiate at ≤520 °C. We hypothesized that a thermolytic temperature lower than 520 °C is not sufficient to initiate the identified mechanistic role of CO_2 in line with homogeneous reactions. To confirm this, a two-stage pyrolysis of SM was performed in a CO_2 environment. The tubular furnace for the external heating source for the pyrolysis experimental work comprises two heating zones, similar to the previous experiments. Accordingly, the temperature of the second heating zone was isothermally set as 650 °C. All experimental parameters (e.g., heating rate of 10 °C min^{-1} and N_2 or CO_2 flowrates of 100 mL min^{-1}) were identical to the one-stage pyrolysis, except the isothermal run in the second heating zone of the furnace. The gaseous effluents from the tubular

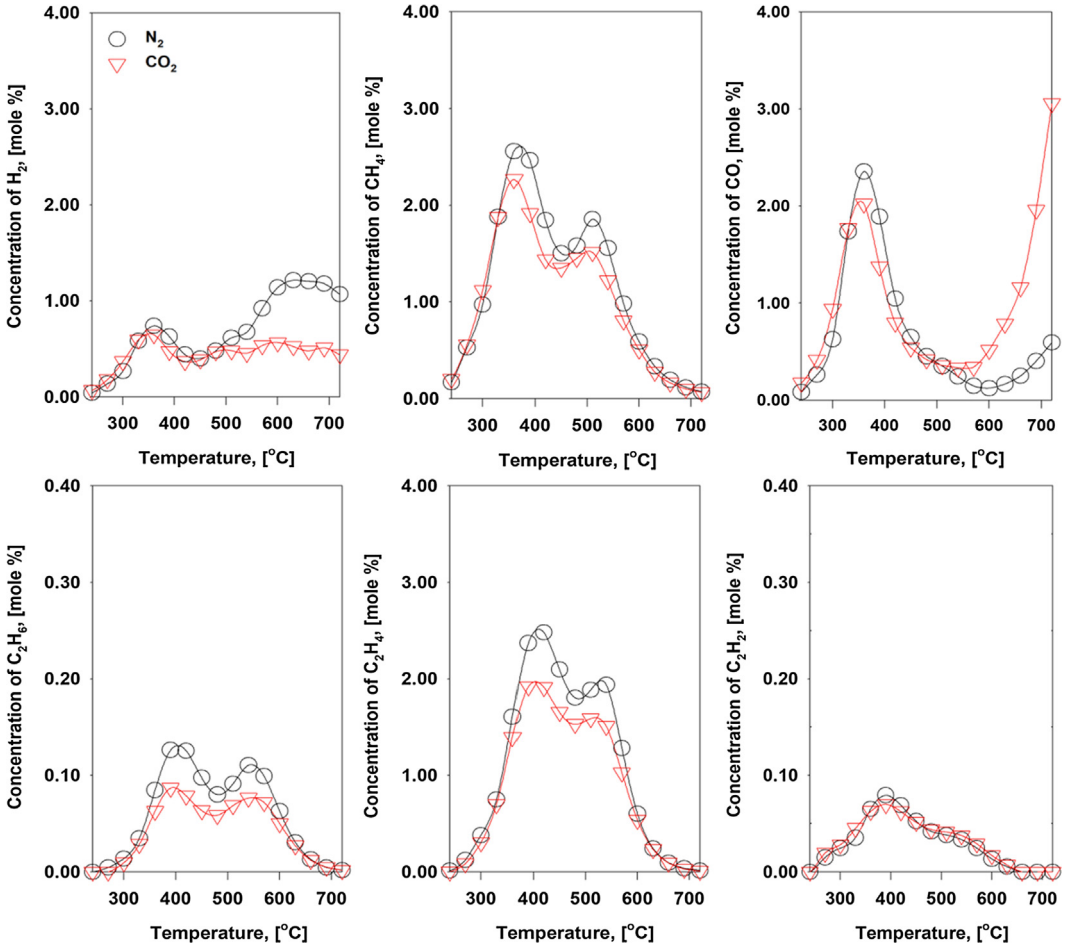

Fig. 5. Concentration profiles of H_2, CH_4, CO, C_2H_6, C_2H_4, and C_2H_2 from two-stage pyrolysis of SM in N_2 (black color) and CO_2 (red color). (For interpretation of the references to colour in this figure legend, the reader is referred to the web version of this article.)

reactor were quantified as a function of thermolytic temperatures, and their concentration profiles are plotted in Fig. 5.

As depicted in Fig. 5, the overall evolution trend is the same as the previous findings in Fig. 4. For example, the enhanced generation of CO begins at ≥520 °C, when the generation of H_2 by dehydrogenation is suppressed. Therefore, all experimental findings from the two-stage pyrolysis are similar to the previous observation from Figs. 2 and 4. To confirm this, the overall mass balance from three-phase pyrolysates from the pyrolysis of SM in N_2 and CO_2 is presented in Fig. 6(a). It can be seen that the mass portions for the biochar samples from N_2 and CO_2 are nearly the same. In contrast, lower amounts of liquid pyrolysates were generated in the CO_2 environment. Moreover, the compositional matrix of the pyrolytic oil was determined using the GC/TOF-MS unit, and their identifications can be visualized in the chromatogram in Fig. 6(b). The major chemical species in Fig. 6(b) were labelled, and their peak areas are summarized in Table 5. All peak areas of

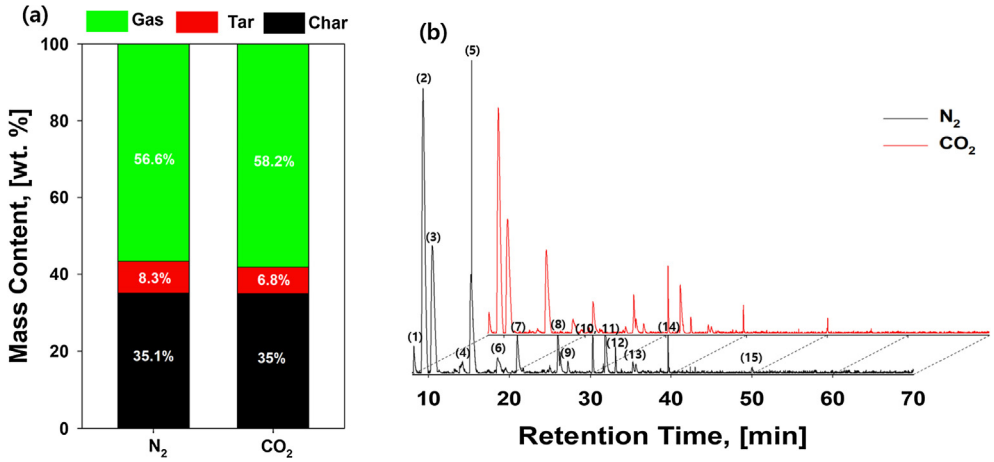

Fig. 6. (a) Overall mass balance of three pyrogenic products evolved from two-stage pyrolysis of SM in the N_2 and CO_2 environments, (b) Identification of the chemical species in pyrolytic oil generated from two-stage pyrolysis of SM in the N_2 and CO_2 environments.

Table 5
Identification of the chemical species in pyrolytic oil generated from two-stage pyrolysis of SM in N_2 and CO_2.

NO.	R.T.	Compound	Peak area from N_2	Peak area from CO_2	Peak area difference (%)
1	8.199	2-propenenitrile	18,523,123	13,192,355	−28.78
2	9.329	chloroform	424,384,588	273,623,736	−35.52
3	10.483	Benzene	214,370,569	160,493,593	−25.13
4	14.21	isopropenyl methyl ketone	18,025,804	4,394,619	−75.62
5	15.349	toluene	177,648,831	104,980,821	−40.91
6	18.563	pyridine	26,849,141	18,341,658	−31.69
7	21.01	styrene	40,049,155	28,820,699	−28.04
8	26.306	acetamide	15,349,157	8,891,474	−42.07
9	27.282	benzonitrile	8,579,443	5,781,547	−32.61
10	30.289	phenol	27,532,693	17,840,416	−35.20
11	31.839	naphthalene	45,154,175	36,220,553	−19.78
12	33.108	p-cresol	12,471,279	6,078,354	−51.26
13	35.271	2-methylnaphthalene	7,810,575	4,639,100	−40.60
14	39.632	1H-indole	11,126,327	6,571,487	−40.94
15	50.012	anthracene	3,274,226	3,070,555	−6.22

condensable pyrolysates from the two-stage pyrolysis of SM in CO_2 are significantly smaller than those in N_2. Therefore, the same explanation in line with the homogeneous reactions can possibly be given. One of the interesting observations in Table 5 is the high content of chemical species containing N. Given that the animal feed especially for a pig contains the large amount of protein, such the N-containing nutrients contribute the formation of chemical species containing N in Table 5.

Accordingly, no homogeneous reactions at $\leq 520\,^{\circ}C$ can be hypothesized due to their slow reaction kinetics. To enhance the reaction kinetics of the homogeneous reactions, SS was loaded as a catalyst in the second heating zone of the tubular furnace. As reported, SS contains numerous metal species which act as catalysts. To confirm this, the gaseous effluent from the two-stage catalytic pyrolysis of SM was analyzed. Note that all experimental parameters are the same as in the case of Fig. 5. As evidenced in Fig. 7, the enhanced generation of CO in the CO_2 environment is observed during the entire temperature regime, which is considered an essential evidence for the aforementioned homogeneous reactions. Moreover, the production of H_2 is substantially suppressed in CO_2, which is consistent with the previous experimental findings. Considering the desire to expedite the reaction kinetics of the homogeneous reactions, all experimental observations strongly suggest that CO_2 can be transformed into CO through homogeneous reactions between condensable pyrolysates and CO_2. In other words, CO_2 is employed as a raw material for the thermo-chemical process, which offers a strategic means for looping CO_2. Nonetheless, process optimization must be developed in the near future.

In addition, SM biochar can be employed for environmental applications (i.e., soil amendment, environmental media, *etc.*) without the environmental burdens. SM contains a large amount of Cu, and the practical use of SM after composting is not realistic due to the high Cu content. Note that the main symptom of toxicity are growth reduction of roots, wilting, and death of shoot tip (Rooney et al., 2006). Furthermore, like toxicities of manganese and zinc, copper toxicity may also induce iron deficiency, which is a conspicuous pale yellow

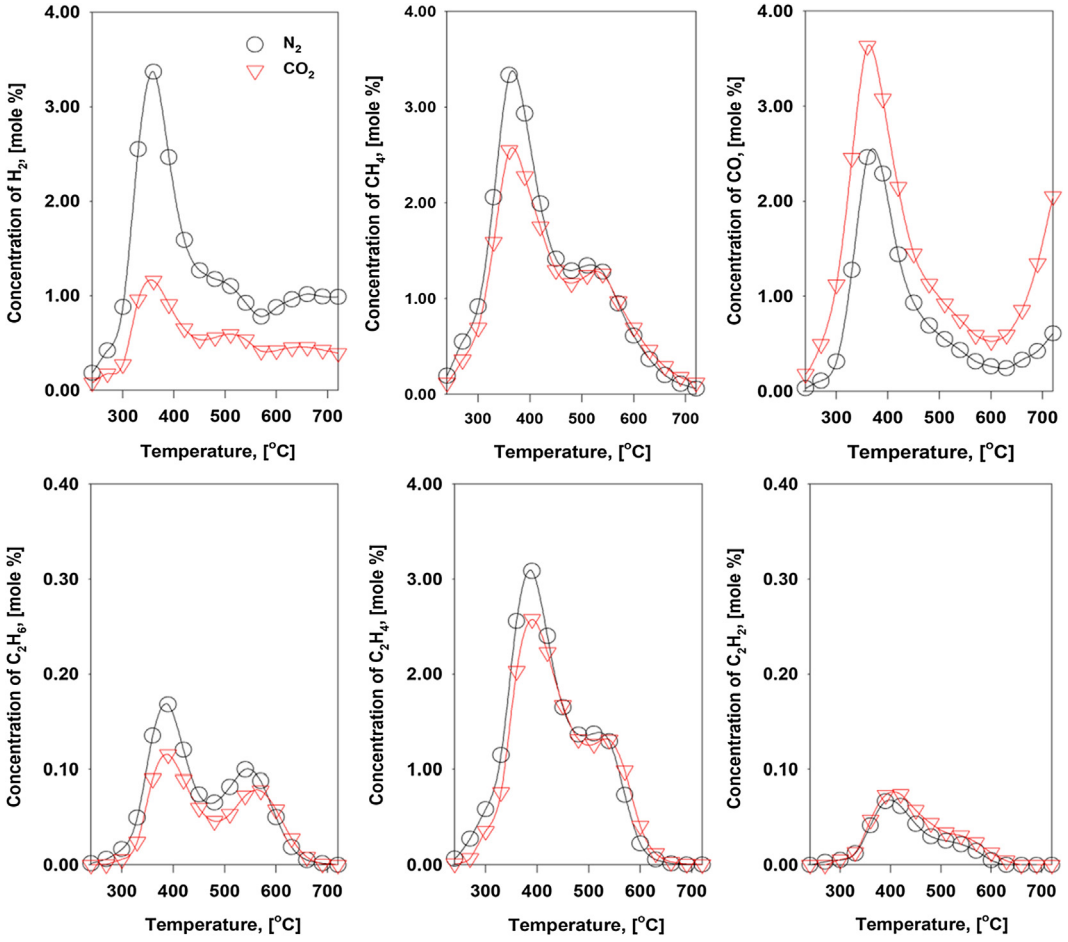

Fig. 7. Concentration profiles of H_2, CH_4, CO, C_2H_6, C_2H_4, and C_2H_2 from two-stage catalytic pyrolysis of SM in N_2 (black color) and CO_2 (red color). (For interpretation of the references to colour in this figure legend, the reader is referred to the web version of this article.)

Table 6
Quantification of metal leaching from the TCLP tests of SM biochar.

Analyte	SM biochar from one-stage pyrolysis in N_2	SM biochar from one-stage pyrolysis in CO_2	SM biochar from two-stage pyrolysis in N_2	SM biochar from two-stage pyrolysis in CO_2
Al	–	–	–	–
Ca	0.53	0.32	0.65	0.55
Cu	–	–	–	–
Fe	–	–	–	–
K	0.94	0.73	0.70	0.67
Mg	0.32	0.63	0.29	0.60
Mn	–	–	–	–
Na	–	–	–	–
Sr	–	–	–	–
Zn	–	–	–	–

intervein chlorosis on the younger leaves (Rooney et al., 2006). In an effort to use SM biochar for the environmental applications, TCLP tests were conducted and their results are summarized in Table 6. Leaching of Cu from the SM biochar is not observed. Therefore, the use of SM biochar without causing environmental burdens may be possible.

4. Conclusions

This study experimentally proved that CO_2 can be used as a raw material in a thermo-chemical process. The homogeneous reactions between volatile pyrolysates and CO_2 resulted in an enhanced generation of CO, with CO_2 acting as an O donor. In parallel, CO_2 effectively suppressed the formation of H_2 by suppressing dehydrogenation. These mechanistic features arising from CO_2 led to a compositional modification of pyrogenic products except for biochar. However, the identified mechanistic role of CO_2 only initiated at $\geq 520\,^{\circ}C$. To expedite the slow reaction kinetics in line with CO_2, SS was employed as a catalyst, which was very effective. Therefore, all experimental findings of this study strongly suggest that CO_2 can be used as a raw material in thermo-chemical processes. Moreover, looping CO_2 is possible in the thermo-chemical process. However, the operational parameters in line with the use of CO_2 should be optimized in the near future. Nevertheless, the identified mechanistic roles of CO_2 from the present study experimentally proved that CO_2 could serve a critical role for restricting the formation of toxic chemicals, such as benzene derivatives and PAHs because CO_2 offered an innovative means for controlling the ratio of C to H_2.

Declaration of Competing Interest

None.

Acknowledgements

This work was carried out with the support of “Cooperative Research Program for Agriculture Science & Technology Development (Project title: Development of optimal liquid fertilization process and utilizing technology for livestock farm, Project No. PJ01268502)” Rural Development Administration, Republic of Korea.

Appendix A. Supplementary material

Supplementary data to this article can be found online at https://doi.org/10.1016/j.envint.2019.105204.

References

Awasthi, M.K., Sarsaiya, S., Wainaina, S., Rajendran, K., Kumar, S., Quan, W., Duan, Y., Awasthi, S.K., Chen, H., Pandey, A., Zhang, Z., Jain, A., Taherzadeh, M.J., 2019. A critical review of organic manure biorefinery models toward sustainable circular bioeconomy: technological challenges, advancements, innovations, and future perspectives. Renew. Sustain. Energy Rev. 111, 115–131.
Balan, V., Chiaramonti, D., Kumar, S., 2013. Review of US and EU initiatives toward development, demonstration, and commercialization of lignocellulosic biofuels. Biofuels, Bioprod. Biorefin. 7, 732–759.
Bilgen, S., 2014. Structure and environmental impact of global energy consumption. Renew. Sustain. Energy Rev. 38, 890–902.
Bortolini, M., Gamberi, M., Graziani, A., 2014. Technical and economic design of photovoltaic and battery energy storage system. Energy Convers. Manage. 86, 81–92.
Burra, K.G., Hussein, M.S., Amano, R.S., Gupta, A.K., 2016. Syngas evolutionary behavior during chicken manure pyrolysis and air gasification. Appl. Energy 181, 408–415.
Chen, C., Pankow, C.A., Oh, M., Heath, L.S., Zhang, L., Du, P., Xia, K., Pruden, A., 2019. Effect of antibiotic use and composting on antibiotic resistance gene abundance and resistome risks of soils receiving manure-derived amendments. Environ. Int. 128, 233–243.
Cséfalvay, E., Horváth, I.T., 2018. Sustainability assessment of renewable energy in the United States, Canada, the European Union, China, and the Russian Federation. ACS Sustain. Chem. Eng. 6, 8868–8874.
Dhillon, R.S., von Wuehlisch, G., 2013. Mitigation of global warming through renewable biomass. Biomass Bioenergy 48, 75–89.
Fatih Demirbas, M., 2009. Biorefineries for biofuel upgrading: a critical review. Appl. Energy 86, S151–S161.
Fuchsz, M., Kohlheb, N., 2015. Comparison of the environmental effects of manure- and crop-based agricultural biogas plants using life cycle analysis. J. Cleaner Prod. 86, 60–66.
Ghaderi, H., Pishvaee, M.S., Moini, A., 2016. Biomass supply chain network design: an optimization-oriented review and analysis. Ind. Crops Prod. 94, 972–1000.
Hashimoto, K., 2019. Global temperature and atmospheric carbon dioxide concentration. In: Hashimoto, K. (Ed.), Global Carbon Dioxide Recycling: For Global Sustainable Development by Renewable Energy. Springer Singapore, Singapore.
Huh, S.-Y., Lee, J., Shin, J., 2015. The economic value of South Korea’s renewable energy policies (RPS, RFS, and RHO): a contingent valuation study. Renew. Sustain. Energy Rev. 50, 64–72.
Hussein, M.S., Burra, K.G., Amano, R.S., Gupta, A.K., 2017. Effect of oxygen addition in steam gasification of chicken manure. Fuel 189, 428–435.
Jang, W.-J., Jeong, D.-W., Shim, J.-O., Kim, H.-M., Roh, H.-S., Son, I.H., Lee, S.J., 2016. Combined steam and carbon dioxide reforming of methane and side reactions: thermodynamic equilibrium analysis and experimental application. Appl. Energy 173, 80–91.
Jung, J.-M., Lee, J., Kim, J., Kim, K.-H., Kwon, E.E., 2016. Pyrogenic transformation of oil-bearing biomass into biodiesel without lipid extraction. Energy Convers. Manage. 123, 317–323.
Kabalci, E., 2013. Design and analysis of a hybrid renewable energy plant with solar and wind power. Energy Convers. Manage. 72, 51–59.
Kahiluoto, H., Kuisma, M., Ketoja, E., Salo, T., Heikkinen, J., 2015. Phosphorus in manure and sewage sludge more recyclable than in soluble inorganic fertilizer. Environ. Sci. Technol. 49, 2115–2122.
Kwon, E.E., Oh, J.-I., Kim, K.-H., 2015. Polycyclic aromatic hydrocarbons (PAHs) and volatile organic compounds (VOCs) mitigation in the pyrolysis process of waste tires using CO_2 as a reaction medium. J. Environ. Manage. 160, 306–311.
Kwon, E.E., Yi, H., Park, J., Seo, J., 2012. Non-catalytic heterogeneous biodiesel production via a continuous flow system. Bioresource Technol. 114, 370–374.
Lardon, L., Hélias, A., Sialve, B., Steyer, J.-P., Bernard, O., 2009. Life-cycle assessment of biodiesel production from microalgae. Environ. Sci. Technol. 43, 6475–6481.
Lee, J., Kim, J., Ok, Y.S., Kwon, E.E., 2017. Rapid biodiesel synthesis from waste pepper seeds without lipid isolation step. Bioresource Technol. 239, 17–20.
Lee, J., Tsang, Y.F., Jung, J.-M., Oh, J.-I., Kim, H.-W., Kwon, E.E., 2016. In-situ pyrogenic production of biodiesel from swine fat. Bioresource Technol. 220, 442–447.
Lee, S.-R., Lee, J., Lee, T., Cho, S.-H., Oh, J.-I., Kim, H., Tsang, D.C.W., Kwon, E.E., 2018. Carbon dioxide assisted thermal decomposition of cattle excreta. Sci. Total Environ. 615, 70–77.
Li, Q., Hu, G., 2016. Techno-economic analysis of biofuel production considering logistic configurations. Bioresource Technol. 206, 195–203.
Meinshausen, M., Meinshausen, N., Hare, W., Raper, S.C.B., Frieler, K., Knutti, R., Frame, D.J., Allen, M.R., 2009. Greenhouse-gas emission targets for limiting global warming to 2 °C. Nature 458, 1158.
Mishra, R.K., Mohanty, K., 2018. Pyrolysis kinetics and thermal behavior of waste sawdust biomass using thermogravimetric analysis. Bioresource Technol. 251, 63–74.
Nizami, A.S., Shahzad, K., Rehan, M., Ouda, O.K.M., Khan, M.Z., Ismail, I.M.I., Almeelbi, T., Basahi, J.M., Demirbas, A., 2017. Developing waste biorefinery in Makkah: a way forward to convert urban waste into renewable energy. Appl. Energy 186, 189–196.
Oh, J.-I., Lee, J., Lee, T., Ok, Y.S., Lee, S.-R., Kwon, E.E., 2017. Strategic CO_2 utilization for shifting carbon distribution from pyrolytic oil to syngas in pyrolysis of food waste. J. CO_2 Utilizat. 20, 150–155.
Prosser, R.S., Sibley, P.K., 2015. Human health risk assessment of pharmaceuticals and personal care products in plant tissue due to biosolids and manure amendments, and wastewater irrigation. Environ. Int. 75, 223–233.
Rooney, C.P., Zhao, F.-J., McGrath, S.P., 2006. Soil factors controlling the expression of copper toxicity to plants in a wide range of European soils. Environ. Toxicol. Chem. 25, 726–732.
Sansaniwal, S.K., Pal, K., Rosen, M.A., Tyagi, S.K., 2017. Recent advances in the development of biomass gasification technology: a comprehensive review. Renew. Sustain. Energy Rev. 72, 363–384.
Sheldon, R.A., 2017. The E factor 25 years on: the rise of green chemistry and sustainability. Green Chem. 19, 18–43.
Stier, P., Hodnebrog, Ø., Myhre, G., Samset, B., Alterskjær, K., Andrews, T., Boucher, O., Faluvegi, G., Fläschner, D., Forster, P., Kasoar, M., Kirkevåg, A., Lamarque, J.-F.,

Olivié, D., Richardson, T., Shawki, D., Shindell, D., Shine, K., Takemura, T., Voulgarakis, A., Watson-Parris, D., 2019. Increased water vapour lifetime due to global warming. Atmos. Chem. Phys. Discuss.
Tomei, J., Helliwell, R., 2016. Food versus fuel? Going beyond biofuels. Land Use Pol. 56, 320–326.
Varun, Bhat, I.K., Prakash, R., 2009. LCA of renewable energy for electricity generation systems—a review. Renew. Sustain. Energy Rev. 13, 1067–1073.
Wigley, T.M.L., Raper, S.C.B., 1987. Thermal expansion of sea water associated with global warming. Nature 330, 127–131.
Xin, Y., Cao, H., Yuan, Q., Wang, D., 2017. Two-step gasification of cattle manure for hydrogen-rich gas production: effect of biochar preparation temperature and gasification temperature. Waste Manage. 68, 618–625.
Yuan, X., He, T., Cao, H., Yuan, Q., 2017. Cattle manure pyrolysis process: kinetic and thermodynamic analysis with isoconversional methods. Renew. Energy 107, 489–496.
Zabed, H., Sahu, J.N., Suely, A., Boyce, A.N., Faruq, G., 2017. Bioethanol production from renewable sources: current perspectives and technological progress. Renew. Sustain. Energy Rev. 71, 475–501.
Zhou, X., Zhou, M., Wu, X., Han, Y., Geng, J., Wang, T., Wan, S., Hou, H., 2017. Reductive solidification/stabilization of chromate in municipal solid waste incineration fly ash by ascorbic acid and blast furnace slag. Chemosphere 182, 76–84.